

C. Thomas Avedisian¹

Sibley School of Mechanical
and Aerospace Engineering,
Cornell University,
Ithaca, NY 14853-7501
e-mail: cta2@cornell.edu

Wei-Chih Kuo²

Sibley School of Mechanical
and Aerospace Engineering,
Cornell University,
Ithaca, NY 14853-7501
e-mail: wk253@cornell.edu

Wing Tsang

Physical and Chemical Properties Division,
National Institute of Standards and Technology,
Gaithersburg, MD 20899
e-mail: wingsang2000@yahoo.com

Adam Lowery³

Sibley School of Mechanical
and Aerospace Engineering,
Cornell University,
Ithaca, NY 14853-7501
e-mail: al659@cornell.edu

High Temperature Thermal Decomposition of Diethyl Carbonate by Pool Film Boiling

We use the configuration of film boiling on a horizontal tube positioned in a stagnant pool of saturated diethyl carbonate (DEC, $(C_2H_5O)_2CO$) to study DEC decomposition at temperatures up to 1500 K. The composition of bubbles that percolate through the liquid pool is measured and the results are used to infer the decomposition reactions. The results show that below tube temperatures of about 1100 K, the decomposition products are ethylene (C_2H_4), carbon dioxide (CO_2), and ethanol ($EtOH$, C_2H_5OH) with a molar ratio $n_{C_2H_4}/n_{CO_2} \sim 1$, which is consistent with a first-order decomposition process. At higher temperatures, $n_{C_2H_4}/n_{CO_2} > 1$ which is explained by an additional route to forming C_2H_4 from radicals in the system (created by $EtOH$ decomposition) attacking DEC. The presence of H_2 , CO , CH_4 , and C_2H_6 in the product stream was noted at all temperatures examined with concentrations that increased from trace values at low temperatures to values comparable to the DEC unimolecular process at the highest temperatures. Formation of a carbon layer on the tube was observed but did not appear to influence the decomposition process. A scale analysis shows that the rate constant controls decomposition compared to the residence time, which has a weaker dependence on temperature. [DOI: 10.1115/1.4038572]

Keywords: film boiling, nucleate boiling, critical heat flux, boiling, boiling heat transfer, reactor, reaction, nucleation, bubble, fuel additive, diethyl carbonate, vapor explosion, lithium, electrolyte

1 Introduction

Film boiling is one of the most important regimes of multiphase heat transfer because of its potential to limit performance in such applications as nuclear reactor meltdown, the metallurgical industry, and cooling of microelectronic equipment [1–3]. The high temperatures that are typical of the film boiling regime can damage the surface on which film boiling is established. And destabilization of film boiling, once established on a hot surface, can lead to vapor explosions [1,4]. Furthermore, gases in the vapor film can react [5–7] and produce combustible products, which is a concern in fusion reactors that involve liquid metals [2] where the molten reactor material may inadvertently contact the coolant (e.g., water) and form hydrogen gases to create a hazardous situation. For these reasons, film boiling is a multiphase heat transfer regime that is typically avoided in industrial processes. On the other hand, film boiling can provide a controlled environment for studying thermal decomposition of organic gases [5–10] and formation of carbonaceous materials [11–14].

In the context of more conventional chemical processing technologies (e.g., packed bed reactor, turbulent flow reactor, jet stirred reactor, shock tube, rapid compression machine, counter-flow flame, etc.), a reactor space developed by film boiling is unique in that it builds itself or is self-assembled. The self-assembly concept is a consequence of creating the reactor volume (Fig. 1) by controlling a process variable (temperature) that transitions the heat transfer modes (essentially automatically) from

nucleate, to critical heat flux (CHF) and finally film boiling where temperatures will be high enough for most organic molecules to fall apart (i.e., decompose). Furthermore, transport of the reactant to the reactor volume is accomplished with no mechanical forcing (e.g., pumps) when under the action of buoyancy. And for organics that are liquid under standard conditions, typical reactors require separate hardware to vaporize the liquid before entering the high temperature reactor space where the reaction occurs. For film boiling, vaporization occurs along with, and not separate from, the evaporation process that gasifies the liquid and supplies the reactant while also sustaining the vapor film.

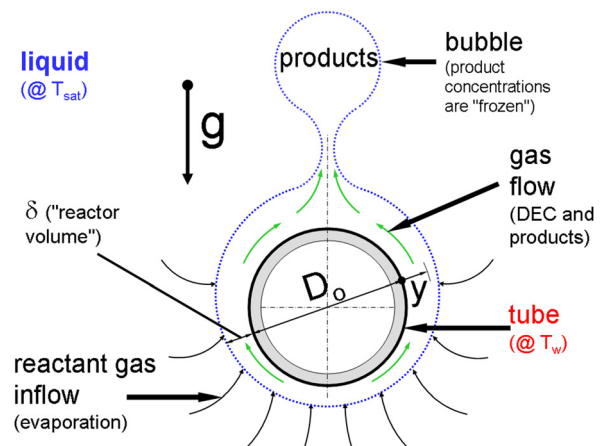


Fig. 1 Schematic of film boiling on a horizontal tube of outside diameter D_o . The gas flow in the vapor film (the “reactor”) is driven by buoyancy and the gases decompose during their transport. Departing bubbles contain decomposition products along with unreacted DEC. This schematic view corresponds to section a–a of the inset photograph in Fig. 4.

¹Corresponding author.

²Present address: CGG, 10300 Town Park Drive, Houston, TX 77072.

³Present address: Department of Mechanical Engineering, Virginia Polytechnic Institute and State University, Blacksburg, VA 24061.

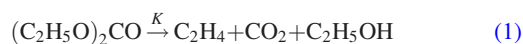
Contributed by the Heat Transfer Division of ASME for publication in the JOURNAL OF HEAT TRANSFER. Manuscript received March 15, 2017; final manuscript received September 19, 2017; published online February 27, 2018. Editor: Portonovo S. Ayyaswamy.

This work is in part a work of the U.S. Government. ASME disclaims all interest in the U.S. Government’s contributions.

In the present study, we show that pool film boiling provides an effective environment to study thermal decomposition of diethyl carbonate (DEC, $C_5H_{10}O_3$, normal boiling point 400 K). Measurements of the product species provide clues to the decomposition mechanism, thereby providing value to film boiling as a viable chemical processing technology. DEC is a useful chemical for this purpose because it is important in various applications such as lithium battery technologies and as an additive to liquid fuels to mitigate formation of particulate matter [15,16]. Furthermore, its decomposition kinetics are rather simple which will facilitate interpreting the results.

As a fuel additive (e.g., to gasoline and diesel fuel), DEC reduces emissions due to oxygen attacking soot precursor species [15,17,18]. Fuel pyrolysis is an important process to the understanding of combustion because the fuel will dissociate at higher combustion temperatures to initiate chain oxidation, and oxidation of a fuel can be influenced by decomposition kinetics of the fuel [15,16]. In lithium-ion batteries, DEC is often mixed with ethylene carbonate to form a solvent for lithium salts to facilitate ion transport between positive and negative electrodes [19]. Rapid charging may lead to electrolyte decomposition by reactions on the electrodes [20,21] at rates that create the potential for thermal runaway and explosions [22–26].

Prior work has shown that DEC decomposition is first-order in the temperature range of 550–700 K [27–31] based on static and flow reactor data. Three species are typically found— CO_2 and C_2H_4 in equimolar proportions, and ethanol (EtOH)—as originally noted in Ref. [32] where DEC decomposition was cast in a class of unimolecular reactions for linear alkyl carbonates



where K is the rate constant for the reaction. An Arrhenius form is often specified for DEC decomposition

$$K = A \exp\left(-\frac{E}{RT}\right) \quad (2)$$

with activation energies determined from experimental results [28–31].

At higher temperatures from shock tube experiments (945–1095 K), these same product gases are found [33], while the temperature is high enough for EtOH as a product of DEC decomposition to itself decompose [33], providing a mechanism for formation of additional species as discussed later. However, the residence times were evidently too short at operational temperatures for EtOH to decompose. DEC decomposition is actually noted to proceed through a two-step sequence: a retro-ene reaction followed by rapid decomposition of alkoxy acid [22,33], as shown theoretically [30] with the overall mechanism being Eq. (1) [29–31,33].

The temperature range previously studied for DEC decomposition is extended in the present study to approximately 1500 K at the upper end. The lower end cannot be below the film boiling temperature of DEC, which is about 700 K for the power-controlled experiments reported here. This temperature range is relevant for the targeted applications (combustion and electrolytic decomposition). At higher temperatures, there can be unique issues associated with decomposition of EtOH (produced by DEC decomposition that remains in the system), which have not been considered in previous studies, that can make the first-order process of Eq. (1) more complicated. Film boiling is used as a comparatively simple way to explore that possibility.

The reactor space for the present study is created on a horizontal tube immersed in a pool of saturated DEC. Figure 1 is a cross-sectional schematic of the film boiling configuration. The tube is positioned in a chamber filled with DEC and heated to transition the heat transfer modes from nucleate boiling to the CHF condition and then to film boiling. Once film boiling is established, the

tube temperature is varied and the contents of the percolating bubbles are chemically analyzed to identify the exhaust gas species as discussed in Sec. 2.

Sections 2 and 3 describe the apparatus and experimental procedures, followed by discussions of the results.

2 Apparatus and Uncertainty

2.1 Apparatus. Figure 2 is a schematic of the apparatus. It consists of a cylindrical sealed glass chamber (4.4 L (ID 150 mm and height: 250 mm) filled with 3.5 L of DEC in the experiments), a horizontally oriented tube on which film boiling is established, condensers filled with dry ice, and a cold trap to further prevent condensable gases from entering the exhaust stream. The condensable products (e.g., mainly EtOH from Eq. (1)) reflux to the liquid pool or are collected in the cold trap. The liquid in the chamber is sampled to determine its composition by withdrawing small volumes from the bottom of the chamber for off-line gas chromatography/mass spectrometry (GC/MS).

Table 1 lists the condensable products detected and their mole fraction in the sealed chamber. The mole fractions are a function of the total liquid volume in the chamber (3.5 L). More importantly are the amounts relative to DEC which are given in the last column. The species in Table 1 are important in the proposed DEC decomposition chemistry (Sec. 3.2). The heater tube assembly consists of a thin-walled nickel-alloy Inconel 600 tube (Micro-Group, Inc. (Miami, FL), # 600F10093X010SL, melting point of 1686 K), 1.85 mm ID, 2.38 mm OD and 80 mm long of which the central 60 mm is the active heating length (electrode clamps are attached to the ends covering approximately 9.5 mm at each end). A tube of this diameter can be considered as almost infinite by the criterion established in Ref. [34]: $D' \equiv D\sqrt{g(\rho_l - \rho_v)/\sigma} > 1$. Using DEC properties, we find that $D' \approx 0.88$.

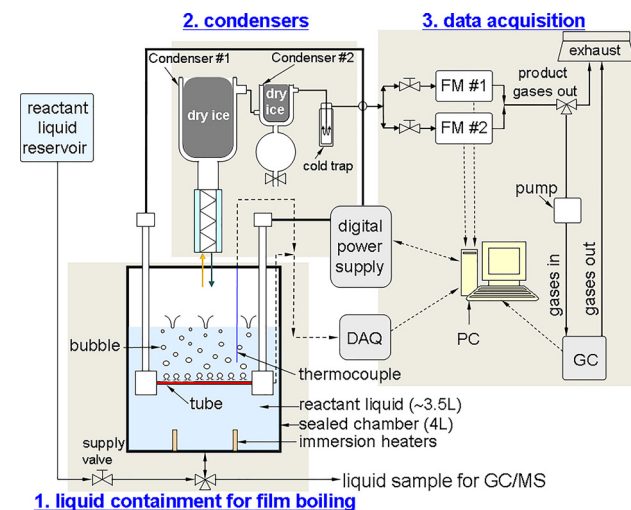


Fig. 2 Schematic of the apparatus

Table 1 Concentrations of the liquid pool after 4 h of continuous operation for $T_w = 1198$ K

Chemical	Formula	T_b (K)	Mole fraction	Relative to DEC
Diethyl carbonate	$(CH_3CH_2O)_2CO$	400	0.8437	1.0
Ethanol	C_2H_5OH	351	0.1432	0.17
Acetaldehyde	CH_3CHO	293	0.0078	0.00924
Water	H_2O	373	0.0051	0.00604
Formaldehyde	CH_2O	254	0.0002	0.00024

To maintain some structural support for the tube, it was internally supported by a ceramic rod (Omega, ORX-132116) to minimize buckling or sagging of the metal when near its softening point at high temperatures. Two thermocouples (Omega, KMQXL-010G) are positioned inside the ceramic tube to measure tube temperature. Corrections for the temperature drop in the radial direction were negligible for conditions of the present experiments [10].

Resistive heating from a DC power supply (Agilent 6681A, 0-8V, 0-580A) interfaced with a LabVIEW controller (National Instruments NI PCI-6281) to a PC provided heat to the DEC in contact with the tube for boiling. The tube is suspended from the top metal flange of the containment chamber by copper clamps connected to 13 mm diameter copper rods passing through the flange and connected to the digital power supply as schematically shown in Fig. 2.

The data acquisition module includes the power supply, two flow meters (Omega, FMA-4310 (FM #1) and FMA-A2309 (FM #2)), a PC, and a gas chromatograph (GC, Gow-Mac Instruments Series 600-TCD gas chromatograph). From the design shown in Fig. 2, the exhaust gases leave the chamber at high temperatures and then cool to ambient as they pass through the condenser section prior to entering the flow meters at atmospheric pressure conditions where their flow is recorded. The flow meters have different ranges to enhance measurement resolution of the product gases. If the gases in the vapor film do not decompose as they flow around the tube, no flow will be registered and the percolating bubbles will contain only the excess DEC that had not decomposed. If no flow is registered, there is no decomposition, which provides a quick check during the experiment that the gases in the vapor film are decomposing. A LabVIEW program controls power to the tube, stores temperatures and gas flow rates, and records the GC output in real time. Calibration curves convert the flow meter output (voltage) to flow rate.

Experiments were performed by controlling power to the tube rather than temperature because of the comparative ease of operation. This option came at the expense of access to the transition boiling regime. The transition (and nucleate boiling) portions of the boiling curves are not of direct interest to the present study because the temperature in these regions is generally too low to promote decomposition at an appreciable rate. Power to the tube was varied in steps by incrementing voltage.

To create film boiling, the Inconel tube is first submerged in the DEC pool and then heated resistively in steps with voltage increments of 0.1 V every 5 min to allow the tube temperature to stabilize. Once film boiling is established, power is varied up to about 1500 K. This method of first flooding the tube prior to a power input is simple, though it will not work for all fluids if the temperature at which DEC achieves film boiling exceeds the melting temperature of the tube material (in this event, another method for developing film boiling can be used to establish film boiling [8]). The transition from nucleate to film boiling is characterized by a rapid temperature excursion. For DEC, the temperature jumps to a low enough value that the tube is not damaged.

The heat flux can be computed from $V \times I/A_s$ where A_s is the surface area over which the tube temperature is uniform. Heat losses through the clamps at the ends resulted in a temperature drop near where the tube is clamped to the electrodes [8–10]. Also, since the voltage is monitored at the output to the power supply and not across the tube itself, there is some uncertainty in the input flux to the liquid by this method.

The alternative is to determine the heat flux from the tube's electrical resistance, $I^2 \times R'/A_s$ ($R' = \rho L/A_s$, where ρ is the temperature-dependent electrical resistivity of Inconel and L is the tube length over which tube temperature is approximately uniform. In this approach, the heat flux is independent of tube length. We assigned a temperature to the flux for the boiling curve to correspond to where the temperature was uniform along the tube axis. In the reported experiments, the tube temperature was uniform over the central 32 mm of the 60 mm section of the tube.

The electrical resistivity used to compute the heat flux was obtained from the supplier of the Inconel 600 tubes [35]. Figure 3 shows the calibration curve relating ρ to T from the available data (known up to about 1200 K). A linear fit was used in the present study to give $\rho(\mu\Omega - m) = 0.99027 + 1.4266 \times 10^{-4} T$ (K) though other correlating approximations are possible. Caution is needed in extrapolating beyond the range of the data. The linear was considered reasonable. As long as the correlating equation for resistivity is known, corrections can always later be made to the flux to accommodate a different correlation or data set for electrical resistivity.

2.2 Experimental Uncertainty. Several sources of uncertainty in the experiment include instrumentation (hardware) precision; and repeatability of the measurements as measured by mean and standard deviations. Manufacturer's specification on instrument accuracy is negligible (for flow meters, power supply (e.g., current accuracy is specified as $\pm 0.1\%$ of the output), and gas chromatograph). More important is the uncertainty associated with the tube temperature, heat flux, product yields, and flow rates of individual species.

Small fluctuations were found for the tube temperature that amounted to less than a few percent about the mean temperature (< 10 K over the range of temperatures in film boiling in Fig. 4). Mechanisms that could be responsible include liquid/solid contact and/or bubble departure cycles that draw in cold liquid to the surface as bubbles depart from the top of the tube to momentarily quench the surface.

Liquid/solid contact in film boiling was noted in some prior film boiling studies [36–39]. Its primary influence is as a precursor to film destabilization. If it occurs in the film boiling regime, DEC would become superheated because the tube temperature is higher than DEC's boiling point of 400 K and contact could potentially result in a sort of rapid evaporation or flash boiling effect that could physically disrupt the vapor film. Visual inspection of the vapor film (cf., note inset in Fig. 4) did not show such an effect. Moreover, the tube temperatures shown in Fig. 4 in the film boiling regime are above the homogeneous nucleation temperature [40] of DEC. It was previously noted [39] that only random small-scale liquid/solid contacts would occur in film boiling under this circumstance, and if so would negligibly influence the overall heat transfer.

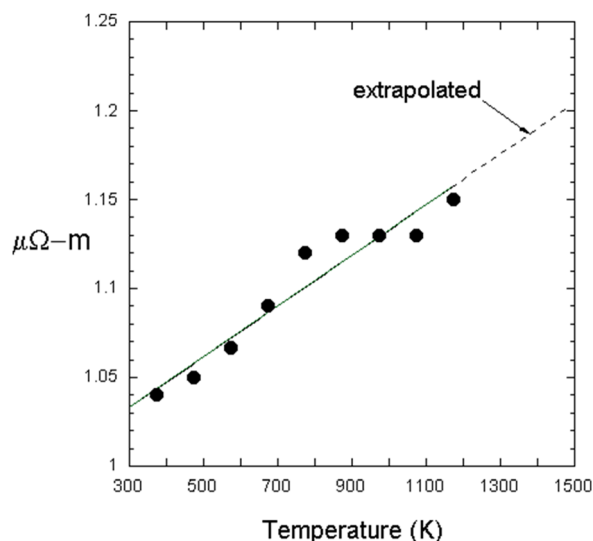


Fig. 3 Calibration of Inconel 600 electrical resistivity with temperature. Data are from Ref. [35] up to 1200 K. Curve-fit is linear, $\rho(\mu\Omega - m) = 0.99027 + 1.4266 \times 10^{-4} T$ (K). Dotted line is extrapolation of linear fit above 1200 K.

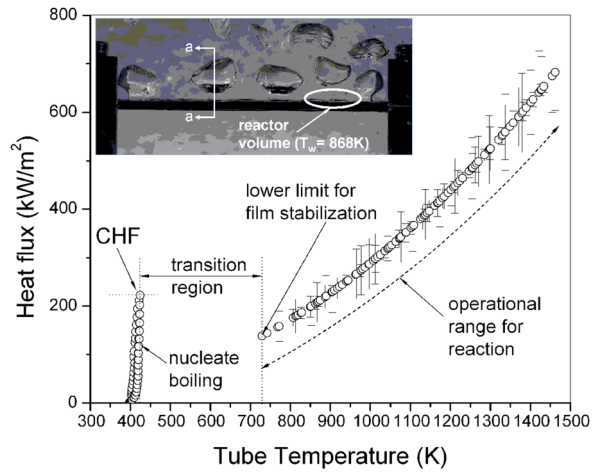


Fig. 4 Variation of heat flux with average tube temperature for DEC. Symbols in the film boiling regime come from a quadratic fit to the heat flux data while the bars indicate standard deviations of the fluxes around the data. The upper temperature is determined by the thermal integrity of the tube material and the lower temperature (as measured in the experiments) corresponds to the onset of destabilization of the film initiated by liquid/solid contacts. The inset is a photograph showing the film boiling configuration at a tube temperature of 868 K. A schematic of section a–a is shown in Fig. 1.

Concerning the uncertainty in power or flux to the tube, there was some scatter of the measured fluxes when repeated under ostensibly the same conditions. To best illustrate this, the measured fluxes ($I^2 \times R'/A_s$) were fitted with a quadratic polynomial. At each average tube temperature associated with a voltage increment, a mean and standard deviation of flux was computed by using the measured current and computed resistivities at the average tube temperature for the voltage increment over the tube length, and the results averaged over the repetitions for each voltage increment. Figure 4 shows the results.

The regularity of the mean fluxes (circles) in Fig. 4 is the result of using the curve-fitted fluxes corresponding to the average tube temperature on the boiling curve. The vertical bars signify the uncertainty of the heat fluxes, which increases with average tube temperature as shown. The maximum standard deviation of heat flux taken as a percent around the mean flux is about 14%.

Regarding uncertainties of the exhaust gas and product species flow rates Fig. 5 shows mean and standard deviations. The scatter is conjectured to be due to bubble departure cycles that create

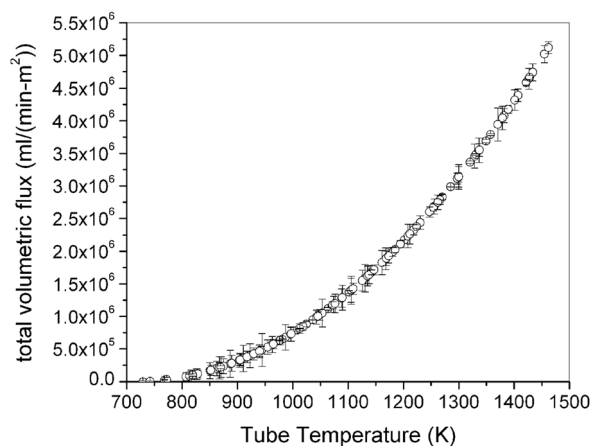


Fig. 5 Variation of total volumetric flux of exhaust gases with temperature. Reaction rate is low below about 700 K, which also coincides with destabilization of the vapor film.

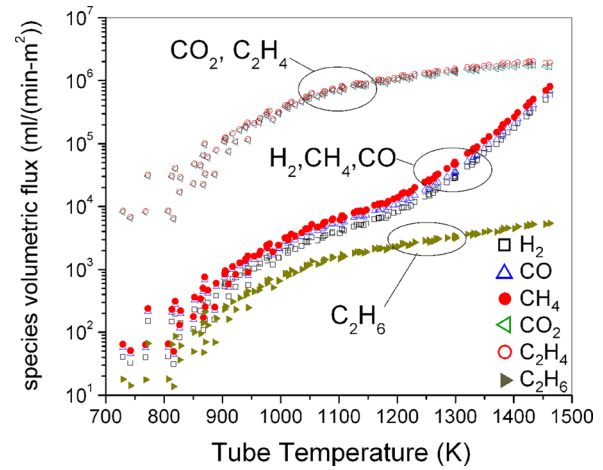


Fig. 6 Volumetric fluxes of noncondensable products in exhaust gas. CO_2 and C_2H_4 are products of DEC decomposition (Eq. (1)). The other species are speculated to form from EtOH decomposition due to radical reactions.

pressure fluctuations in the space above the free liquid surface as bubbles intermittently break through it. Furthermore, the product flow rates of the stable species detected in the exhaust gas are derived from the GC output and the total gas flow rates. As a result, the uncertainty in the individual species flow rates shown in Fig. 6 should be similar to uncertainties in total gas flow rates (Fig. 5).

Regarding Fig. 6, individual species flow rates are shown without means and standard deviations in order to unclutter the figure and better illustrate trends. The species flow rates exhibit considerable scatter below about 900 K due to instrumentation limitations. For ethane, in particular, the flow rates are an order of magnitude below H_2 , CH_4 , and CO at tube temperatures below about 900 K. At higher temperatures, the differences approach almost three orders of magnitude as ethane formation enters a region where its concentration is almost independent of temperature while the other product concentrations continue to increase with temperature. The low concentrations of ethane reflect the apparent unimportance of ethane in the overall decomposition of DEC. Nonetheless, in Sec. 3.2, we offer a more complex DEC decomposition mechanism as an alternative to the relatively simple one of Eq. (1) to explain the routes by which all of the product gases shown in Fig. 6 may form.

An additional uncertainty is the temperature at which the decomposition reaction occurs. Appendix A considers this matter. This concern is due to the large temperature drop from the tube surface to the liquid/vapor interface. To address this concern, the reaction temperature for film boiling is framed in terms of a threshold value that essentially defines a sublayer within the vapor film, close to the tube surface, where most of the reactant gases would decompose. As shown in Appendix A, and based on DEC's activation energy, a sublayer within which DEC would supply 90% of its decomposition products (by Eq. (1)) to the exhaust stream would have a temperature at the other edge within a few degrees of T_w . This implies that the remaining 10% of the product gases would come from decomposition at lower temperatures outside of this higher temperature sublayer. In the presentation of the results that follows, the average tube temperature (T_w) is used as a reference value with this consideration in mind.

3 Results

3.1 Boiling Curve. The operational domain of the film boiling configuration in Fig. 1 is determined by the boiling curve of a liquid. The boiling curve relates the heat flux to the fluid with the temperature of the surface that dissipates the heat. Figure 4 shows the measured boiling curve for nearly saturated DEC at 400 K.

The photograph in the inset shows the film boiling bubble morphology at $T_w = 868$ K. The section indicated as “a-a” corresponds to Fig. 1.

The film boiling regime is marked by the dotted curve, which is the operational domain for chemical reaction. It is bounded at the lower end by the minimum film boiling temperature below which the vapor film cannot be stabilized and at the upper end by material considerations for the surface on which film boiling is supported (e.g., the softening point of the material).

Quantitative predictions of the various regimes of the DEC boiling curve are difficult to make because available predictive formulations are largely empirically based. For example, for nucleate boiling, an “empirical correction factor for surface conditions” is required [34], which is not known for DEC. Correlations for the film boiling heat transfer coefficient [34] incorporate fitted constants obtained from data for a range of fluids though DEC data are not among them. And, minimum film boiling heat flux formulations include an “arbitrary constant” [34], which is essentially a variable that correlates the data.

The CHF has a more rigorous foundation and we apply it to predict the CHF indicated in Fig. 4. The CHF mechanism is based on coalescence of bubble streams formed where the Taylor wavelength becomes unstable and liquid return to the surface is choked by Helmholtz instabilities in the bubble streams. For a horizontal cylinder, Eq. (9.18) of Ref. [34] is relevant. DEC property data evaluated at 424 K (the DEC surface temperature at CHF) give a predicted CHF using this formulation of 245 W/m^2 , which is close to the value in Fig. 4 (221 W/m^2).

An example of the transition from nucleate boiling to film boiling for DEC is shown in Supplemental Video, which is available under the “Supplemental Data” tab for this paper on the ASME Digital Collection. The bulk liquid temperature is 397 K ($T_{\text{sat}} = 400$ K for DEC). The location for initiating film boiling was found to be somewhat random in the experiments. In the posted video, film boiling originates on the right side near where the tube is clamped to the electrodes and moves to the left. A red arrow marks the transition from nucleate to film boiling. Across the transition from nucleate to film boiling, the tube surface temperature increases from about $T_w = 424$ K to about 943 K, which illustrates the strong insulating effect of the vapor film. Selected images from this video are also shown, which track the interface and development of film boiling.

3.2 Product Yields and Flow Rates. Figure 5 shows the variation of total exhaust gas volumetric flux ($\text{ml}/(\text{min m}^2)$) with average tube temperature in the film boiling regime. The exhaust gases are a mixture of noncondensable products formed from decomposition. The trends show that above about 1000 K the volumetric fluxes start to increase monotonically with temperature, which reflects the dependence of the rate constants (e.g., Eq. (2)) for the various reactions on temperature. At the lowest tube temperatures (< 800 K), the flow rate is still nonzero because decomposition will occur at any temperature (e.g., Eq. (2) as a rate constant) though it does not show up on the scale of Fig. 5. Estimates of measurement uncertainty are included in Fig. 5. The estimates were obtained by taking the difference between a second-order polynomial curve-fit of the data and the measured rates at each temperature.

From the total flow rate data, and knowing the distribution of the components from GC analyses (i.e., the molar concentrations of species in the gas mixture), the volumetric fluxes of each component can be obtained. Figure 6 shows the volumetric fluxes of the individual species in the exhaust stream. The data in Fig. 6 result from curve-fitting species mole fractions (obtained from analyzing GC traces) with tube temperatures and then multiplying the fitted mole fractions at selected temperatures by the total volumetric flux data in Fig. 5. There is significant scatter in the concentrations below about 1000 K due to the resolution of the flow meter though the data are more reliable at higher tube temperatures. It is clear that CO_2 and C_2H_4 have the highest volumetric fluxes below about 1300 K (by two orders of magnitude) relative

to other species in the produce stream, which would be in keeping with Eq. (1) as the main decomposition route for DEC. However, at higher tube temperatures, the presence of H_2 , CO , CH_4 , and C_2H_6 in the exhaust gas and the progressive increase of their concentrations with temperature suggests competing influences on DEC decomposition, which cannot be explained by Eq. (1) alone. In the discussion below, we offer a series of reactions to explain formation of these additional species. We believe they are the result of unstable radicals in the vapor film reacting with DEC as an alternative path to DEC conversion by Eq. (1). The radicals themselves are considered to form by decomposition of EtOH (which is viable above about 700 K [41]) and that EtOH gets into the vapor film by preferential vaporization of refluxed EtOH from the DEC/EtOH mixture or by forming naturally by Eq. (1) as gases flow and decompose in the vapor film.

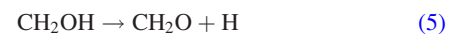
The radicals of interest include CH_3 (methyl), H (hydrogen), OH (hydroxy), HCO (formyl), CH_2OH (hydroxymethyl), and $\text{C}_2\text{H}_4\text{OH}$ (2-hydroxyethyl). For example, decomposition of EtOH can form CH_2OH and $\text{C}_2\text{H}_4\text{OH}$ along with methyl radicals by



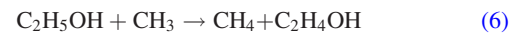
and



H atoms can be produced by decomposition of the hydroxymethyl radical



where we know that formaldehyde (CH_2O) is present in the system (Table 1). Two sources of methane are



(at high temperatures) and



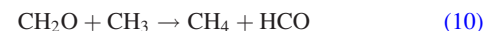
(at low temperatures) which can recombine as the source of ethane



An additional source of ethylene (besides DEC decomposition) is decomposition of the 2-hydroxyethyl radical



HCO could be produced by any of



(which is another source of methane besides Eqs. (6) and (7))



(another source of hydrogen besides Eq. (5)) and



HCO is unstable and will decompose to



which adds more hydrogen atoms to the system and is the source of carbon monoxide.

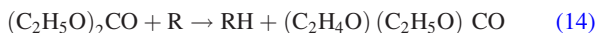
The stable product species increase with temperature as shown in Fig. 6. The precise form of these variations cannot be determined quantitatively merely by listing reactions that factor into

their formation. A detailed kinetic analysis that employs rate constants is required. Broadly viewed, the increase of concentrations with temperature is consistent with the strong dependence of the rate constants on temperature for the reactions that would form them (see Appendix B).

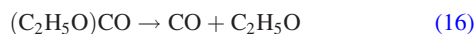
Figure 6 shows a significant upturn in methane volumetric flux in the tube temperature range of 1000–1200 K at the about the same temperature that ethane begins to level off. Considering the importance of methyl radicals in formation of both molecules (Eqs. (7) and (8)), if CH_3 is more prone to react with H atoms (Eq. (7)) than recombine to form ethane (Eq. (8)), then the increasing production of methane above 1200 K would come at the expense of ethane with a compensating effect of a reduced sensitivity of the ethane concentration on temperature.

The concentrations of CO_2 and C_2H_4 increase with temperature below about 1000 K as shown in Fig. 6, then become almost independent of temperature at 1450 K. This increase at low temperatures is consistent with the strong dependence of rate constant on temperature. The leveling off of concentrations at high temperatures is more speculative and illustrates the importance of radicals in the system (versus stable species).

Radicals formed by EtOH decomposition (the presence of which in the vapor film arises from refluxed and preferentially vaporized EtOH or formed in the vapor film by Eq. (1)) could attack DEC. This possibility could result in formation of other species besides CO_2 and C_2H_4 at high temperatures, for example by



where “R” could be H, OH, and/or CH_3 . Acetaldehyde ($\text{C}_2\text{H}_4\text{O}$) is present in the liquid pool (Table 1) as a refluxed condensable product of decomposition. For $\text{R} = \text{OH}$ we would have $\text{RH} = \text{H}_2\text{O}$, for $\text{R} = \text{H}$ then $\text{RH} = \text{H}_2$ on the right-hand side, and for $\text{R} = \text{CH}_3$ then $\text{RH} = \text{CH}_4$. These stable (“RH”) species increase their concentrations in the vapor film, which supports the upturn in concentrations shown in Fig. 6 at high temperatures (i.e., in the 1000–1200 K range as shown in Fig. 6). Concerning the second group on the right-hand side of Eq. (14), the following reactions are plausible:



Equation (15) may not be important at high temperatures because it adds ethylene to the system while Fig. 6 shows that ethylene reaches a sort of plateau (though the difference with CO_2 increases). On the other hand, Eq. (16) can add CO at high temperatures. Figure 6 shows an increase of CO above about 1200 K, which could be due to Eq. (16) adding to the concentration of CO in addition to Eq. (13). And Eq. (17) adds methyl radicals, which favor formation of methane (Eq. (8)) which also show an upturn above 1200 K.

The formation of ethane comes from the methyl (i.e., CH_3) radical recombination reaction of Eq. (8). At the same time, CH_3 also has an affinity for H atoms to form methane by Eq. (7). At low temperatures reactions with H atoms (Eq. (7)) and the recombination reaction of Eq. (8) both occur such that $n_{\text{C}_2\text{H}_4} > n_{\text{CO}_2}$ as suggested in Fig. 6 below about 1000 K. Between 1000 K and 1200 K, the rate of formation of ethane clearly decreases while methane increases and the concentrations diverge. The concentration of C_2H_6 becomes almost independent of temperature. We attribute this trend to the shifting affinity CH_3 has for H atoms as temperature is increased such that CH_3 radicals will have a greater propensity to react with H atoms (Eq. (7)) rather than recombine with itself (Eq. (8)) to form ethane. This shift depletes the system

of ethane so its concentration levels off while the concentration of methane increases as the reaction rate of Eq. (7) increases substantially with increasing temperature.

The concept of a reactor “residence time” (t_r) is an often employed metric to characterize a reactor’s ability to promote conversion of chemicals of interest. For a film boiling reactor, the residence time is related to process variables such as gas velocity, temperature, gravity, and tube size. Additionally, the rate constant (K) for a reaction (e.g., Eq. (2)) is a crucial parameter. It is shown in Appendix B that the product of residence time and reaction rate is proportional to the decomposition rate of reactant, $K \times t_r$, where

$$t_r \sim \left(\frac{\rho_v \text{Pr}}{\rho_L - \rho_v \text{Ja}} \right)^{1/2} \left(\frac{D}{g} \right)^{1/2} \quad (18)$$

With Eqs. (2) and (18), the concentration of reactant for a unimolecular process is then proportional to

$$K \times t_r \sim A \exp\left(-\frac{E}{RT}\right) \times \left(\frac{\rho_v \text{Pr}}{\rho_L - \rho_v \text{Ja}} \right)^{1/2} \left(\frac{D}{g} \right)^{1/2} \quad (19)$$

Equation (19) shows the competing influences of temperature (temperature appears in the Jakob number, Ja). The rate constant increases exponentially with increasing temperature in K while the residence time decreases with increasing temperature, which reduces the probability that a reactant molecule will decompose at the prevailing conditions. From Figs. 5 and 6, it is evident that the exhaust and individual species volumetric fluxes increase with temperature so that kinetics control decomposition.

Comparing $n_{\text{C}_2\text{H}_4}$ with n_{CO_2} provides a clue to the importance of Eq. (1) as the main decomposition route for DEC. From Fig. 6, the concentrations for both overlap over the range of tube temperatures investigated, which would be consistent with first-order DEC decomposition according to Eq. (1). Figure 7 more clearly distinguishes the molar ratios, $n_{\text{C}_2\text{H}_4}/n_{\text{CO}_2}$ with tube temperature from the data in Fig. 6. It is seen that $n_{\text{C}_2\text{H}_4}/n_{\text{CO}_2} \approx 1$ below about 1200 K. Since CO_2 only forms by Eq. (1) for the decomposition mechanism we propose the increase of $n_{\text{C}_2\text{H}_4}/n_{\text{CO}_2}$ substantially above unity could come by adding C_2H_4 to the system. EtOH decomposition provides this possibility. For example, the 2-hydroxyethyl radical formed by Eq. (6) can subsequently decompose (Eq. (9)) at high temperatures to produce more C_2H_4 .

As a final consideration of the experimental results, we note formation of a layer of solid deposits on the tube over time. Figure 8(a) shows a scanning electron micrograph (SEM) image of an Inconel tube after an experiment. Solid deposits on the surface are evident.

The mechanism by which carbon can form are complex and speculative. The role of ethylene on carbon formation has been

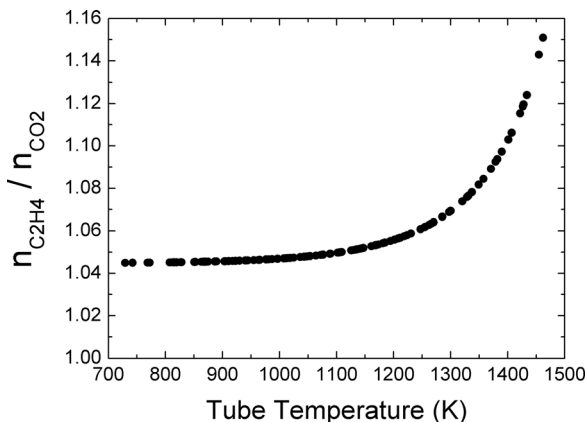


Fig. 7 Variation of $[\text{C}_2\text{H}_4]/[\text{CO}_2]$ (data from Fig. 7) with tube temperature (K)

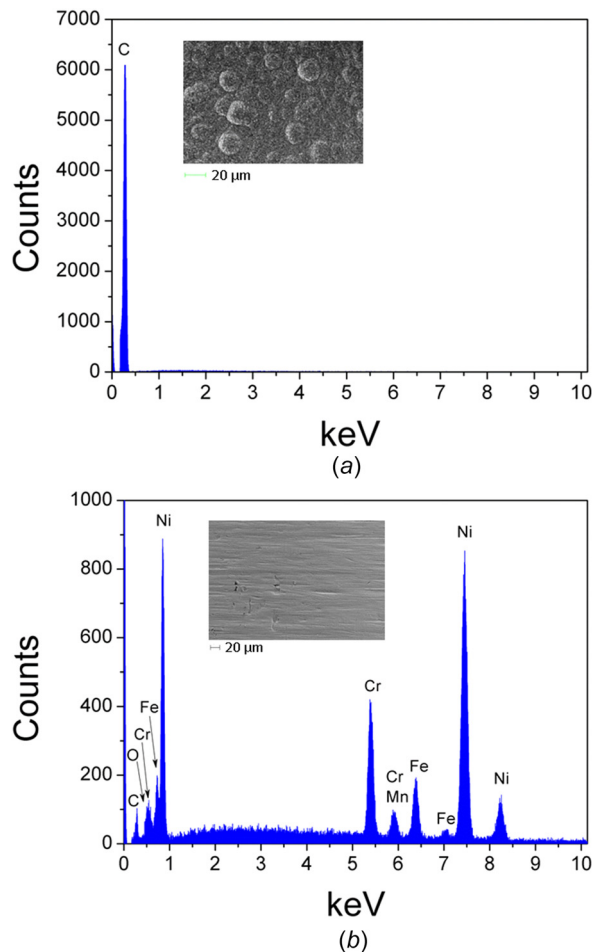


Fig. 8 (a) EDX analysis of a carbon flake with insert SEM image and (b) EDX analysis of a bare tube with SEM image shown in inset

recognized and it appears to be prevalent at temperatures above about 850 K [42]. At high temperatures ethylene can polymerize and lead to formation of coke through a process broadly represented as $C_2H_4 \rightarrow \text{olefins} \rightarrow \text{polymers} \rightarrow \text{carbon}$.

Energy-dispersive X-ray spectroscopy (EDX) analysis was used to determine the composition of the deposits. Figure 8(a) shows them to be pure carbon. With formation of a carbon layer, the surface morphology changes during an experiment from being smooth for a clean tube prior to being used in an experiment (Fig. 8(b)) to a more roughened configuration (Fig. 8(a)) as shown by the SEM images. The EDX analysis of a bare Inconel tube shows it to be comprised of nickel, chromium, and iron as the major constituents as expected for Inconel 600 [35]. Even though carbon coats the tube over time, the results showed no significant change in the product gas flow rates. Nonetheless, a new (clean and polished) tube was employed for each experiment. The mechanisms for forming carbon by surface reactions are not well established. The role of ethylene has been noted at temperatures above about 850 K [42] where it can polymerize and form carbon or coke through a process broadly represented as $C_2H_4 \rightarrow \text{olefins} \rightarrow \text{polymers} \rightarrow \text{carbon}$.

4 Summary

The configuration of film boiling on a horizontal tube in a saturated pool of DEC was used to study DEC decomposition at temperatures up to 1500 K. The results are summarized as follows:

- (1) Below about 1100 K, the decomposition products were mainly ethylene (C_2H_4), carbon dioxide (CO_2), and ethanol

(EtOH, C_2H_5OH) with $n_{C_2H_4}/n_{CO_2} \approx 1$, thus corresponding to a first-order decomposition process for DEC in this temperature range.

- (2) Above about 1200 K $n_{C_2H_4}/n_{CO_2} > 1$, which is explained by an additional route to forming C_2H_4 from DEC being attacked by the radicals formed by EtOH in the film. The additional species found in the product stream were hydrogen (H_2), carbon monoxide (CO), methane (CH_4), and ethane (C_2H_6) predominantly at high temperatures, as below 1200 K their concentrations were in trace quantities.
- (3) Formation of a carbon layer on the tube was observed but did not appear to influence the decomposition process.
- (4) A scale analysis suggests the role of kinetic and transport mechanisms on DEC decomposition. It is shown that the rate constant should control decomposition compared to a residence time effect because the rate constant is exponentially dependent on temperature and increases with temperature, while the residence time is algebraically dependent and decreases with increasing temperature.
- (5) The product noncondensable gases in highest concentrations were ethylene (C_2H_4) and carbon dioxide (CO_2) at nearly equal concentrations below 1200 K though in very low concentrations compared to ethylene and carbon dioxide. Refluxed ethanol (EtOH) was also found in the liquid pool. These observations are consistent with a first-order unimolecular decomposition for DEC.
- (6) The tube temperature is a reasonable measure of the reaction temperature at low tube temperatures though it becomes less so as tube temperature increases.
- (7) A DEC decomposition mechanism is proposed that is more complicated than the unimolecular process which produces only ethylene, carbon dioxide and ethanol. It is considered to be relevant to tube temperatures above about 1200 K where the noncondensable gas concentrations approach that of ethylene and carbon dioxide. The mechanism centers around ethanol decomposing to form radicals that then react with other molecules. The mechanism accounts for all of the stable noncondensable gases detected.

Acknowledgment

We thank Dr. Xia Zeng of the Human Ecology Department at Cornell for the GC/MS analysis, Mr. Pushan Sharma of Cornell for some discussions, and Mr. Malcolm Thomas for the EDX analysis of carbon deposits.

Funding Data

- National Science Foundation with Dr. Jose Lage as the Program Manager (Grant No. CTS-1336657).

Nomenclature

- A = frequency factor for rate constant, Eq. (2)
 A_s = tube surface area, $\pi D_o L$
 A_x = tube cross-sectional area $\pi(D_o^2 - D_i^2)$
 c_{pv} = gas specific heat
 D_i = tube inside diameter
 D_o = tube outside diameter
 E = activation energy
 g = gravitational constant
 Ja = Jakob number, $(c_{pv}(T_w - T_{sat}))/h_{fg}$
 K = rate constant
 k_v = gas thermal conductivity
 L = tube length
 $n_{C_2H_4}$ = number of moles of ethylene
 n_{CO_2} = number of moles of carbon dioxide
 Pr = Prandtl number, $\mu_v c_{pv}/k_v$
 r = radial coordinate ($D_i/2 \leq r \leq D_o/2 + \delta$), Fig. 11

R' = material electrical resistance
 R = gas constant
 T = temperature
 T_{sat} = saturation temperature or normal boiling point
 T_t = threshold temperature corresponding to ε
 T_w = average tube surface temperature
 y = coordinate measured from tube surface ($0 \leq y \leq \delta$) Fig. 9

Greek Symbols

δ = vapor film thickness
 δ_t = reaction sublayer in the vapor film, Fig. 9
 ε = conversion at T_t relative to conversion at T_w
 θ = angular coordinate, Fig. 11
 μ_v = gas viscosity
 ρ = tube electrical resistivity, Fig. 3
 ρ_L = liquid density
 ρ_v = gas density
 $[...]$ = denotes concentration of species within brackets

Appendix A: Reaction Temperature

The nonuniform temperature within the vapor film in the film boiling regime complicates specifying a reaction temperature for decomposition. The large temperature gradient within the vapor film provides some spatial confinement to decomposition due to the strong dependence of reaction rate on temperature. This appendix analyzes the potential for the temperature gradient to spatially confine decomposition within the vapor film to facilitate specifying an average temperature within the layer as a suitable reaction temperature.

Temperature varies across δ from T_w at the tube surface to T_{sat} at the liquid/vapor interface. Figure 9 is a schematic of the temperature variation for a linear temperature distribution [5,43,44]

$$T = T_w + (T_{\text{sat}} - T_w) \frac{y}{\delta} \quad (\text{A1})$$

Homogeneous decomposition occurs throughout δ . The highest contributions from decomposition of the reactant to the exhaust stream will come from a sublayer with the highest temperatures—close to the tube surface), because of the dependence of the rate constant (Eq. (2)) on temperature.

Assuming that kinetics control decomposition we define a fractional conversion at a threshold temperature T_t relative to T_w as

$$\varepsilon(T) = \exp\left(-\frac{E}{R} \left\{ \frac{T_w - T_t}{T_w T_t} \right\}\right) \quad (\text{A2})$$

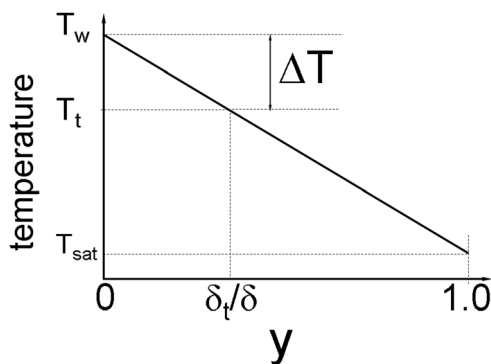


Fig. 9 Schematic of temperature variation across δ . T_t is a threshold temperature defined by ε (Eq. (A2)) and δ_t is the corresponding reaction boundary layer that supplies product gases from decomposition. The product species are formed mainly over $y < \delta_t/\delta$ at an average temperature within this layer while the remaining supply of product gases comes from $\delta_t/\delta < y < 1$.

where T_t is the temperature at the edge of the reaction layer (δ_t) corresponding to ε . Within this sublayer or inner zone ($0 < y < \delta_t$) the product gases would be supplied by decomposition at an average temperature within $\Delta T = T_w - T_t$. Below the selected ε (i.e., over the region $\delta_t < y < \delta$ or in an outer zone) reactant gases would be exposed to temperatures less than T_t and therefore yield products at a lower rate compared to the inner zone.

The variation of ε with y is illustrated in Fig. 9(a) for the linear temperature distribution (Eq. (A1)). The activation energy was taken from Ref. [30] ($E \approx 194$ kJ/mol). The sharp decrease of ε from the tube surface ($y = 0$) reflects the strong dependence of K on temperature. If, for example, we base a reaction temperature on $\varepsilon = 0.9$, and consider the case $T_w = 800$ K. Eqs. (A1) and (A2) show that 90% of the product gases will be supplied by decomposition within the thin layer $0 < y/\delta_t < 0.0072$ ($=\delta_t/\delta$). The remaining 10% of the products would form within $\delta_t/\delta < y/\delta < 1$. For this case it would be reasonable to assign T_w as the reaction temperature because for $\varepsilon = 0.9$, $T_t = 797$ K.

To further illustrate the potential for T_w to be a reasonable measure of the thermal state of a decomposition reaction by film boiling under some circumstances, Fig. 10(b) shows the variation of ΔT with ε for three values of T_w . As an example, the simulation shows that 99% of the DEC conversion to products by Eq. (1) will occur within about 100 K of T_w when $T_w = 800$ K. For $\varepsilon = 0.90$ and $T_w = 800$ K, 90% of the conversion of DEC to products occurs

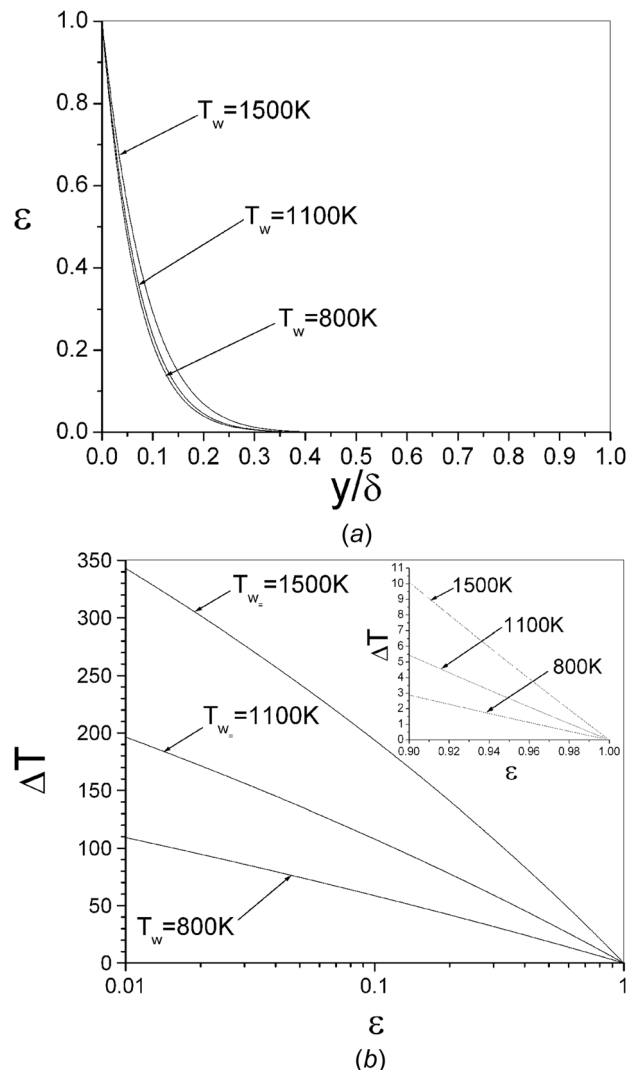


Fig. 10 (a) Variation of ε across the vapor film for Eq. (1) corresponding to the indicated T_w and (b) variation of $\Delta T = T_w - T_{mr}$ with ε . Inset expands the scale around $\varepsilon = 1$.

within about 3 K of T_w (average reaction temperature half this value) which is more clearly shown in the inset to Fig. 10(b) which expands the scale around $\varepsilon = 1$.

Appendix B: Residence Time in Film Boiling

The residence time (t_r) is fundamentally a measure of the time it takes for a molecule to reach a vibrational state where it would have a high probability of falling apart or decomposing. It is possible to theoretically predict such probabilities [45], though it is outside the scope of the present study to do so. Instead, we interpret the residence in a different way to evaluate the trends.

In film boiling we take the residence time as the time for a fluid element to traverse the circumference of the tube on which film boiling is established. For a fluid velocity V

$$t_r \sim \frac{D}{V} \quad (\text{B1})$$

where the $\pi/2$ factor is dropped because we are only interested in an order of magnitude. The velocity, which is controlled entirely by buoyancy here, is the controlling process variable. Before turning to an estimate of V , we place t_r in the context of a decomposition reaction to illustrate its importance in the decomposition process.

Assuming a unimolecular process as given by Eq. (1), a general decomposition reaction is



The rate of conversion of A determines the effectiveness of the reactor design. For Eq. (B2) the law of mass action relates the concentration of A (denoted by “[A]”) to the rate constant K as

$$\frac{d[A]}{dt} = -K[A] \quad (\text{B3})$$

Assuming for simplicity that the temperature within δ does not depend on time, Eq. (B3) can be integrated from an initial concentration $[A]_i$ to $[A]$ over the time 0 to t_r to give

$$\log [A]_i - \log [A] \sim K \times t_r \quad (\text{B4})$$

Equation (B4) shows that both K and t_r influence conversion. Equation (2) shows a strong dependence of K on temperature and the energy barrier to the reaction. For t_r we do not know how variables influence it. We now turn to predicting t_r .

The interest is less in developing a quantitative predictive capability for t_r than to determining the variables on which it depends. A scaling approach is appropriate to this end. We use it to “solve” the momentum equation for velocity, and use an energy balance across the vapor film to relate δ to parameters. Figure 9 is a schematic diagram showing the coordinates for scale analysis to determine the buoyant gas velocity and thereby t_r from Eq. (B1).

The problem of determining t_r is formulated in analogy to the Nusselt theory of laminar film condensation [34] in which it is assumed that $\delta/R \ll 1$ and the inertia terms can be neglected in the momentum equation [5,43,44]. Fluid friction is then balanced by buoyancy and the momentum equation simplifies to (see Fig. 11)

$$\mu_v \frac{\partial^2 V}{\partial y^2} + g(\rho_L - \rho_v) = 0 \quad (\text{B5})$$

We employ the scalings $V \sim V_B$, $y \sim \delta$ and $(\partial^2 V / \partial y^2) \sim (V_B / \delta^2)$ to solve for the velocity in Eq. (B5) as

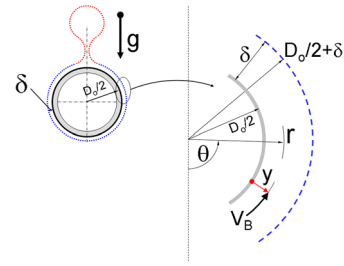


Fig. 11 Schematic of vapor film showing the coordinates for scale analysis to determine the buoyant gas velocity (V_B), residence time (t_r), and vapor film thickness (δ). δ is shown as nearly constant though in reality it varies with θ .

$$V_B \sim \frac{\delta^2 g (\rho_L - \rho_v)}{\mu_v} \quad (\text{B6})$$

An energy balance on the vapor film (neglecting radiation) equates conduction across the film to the energy needed for evaporation

$$k_v A_s \frac{\partial T}{\partial y} \sim \dot{m} h_{fg} \quad (\text{B7})$$

where $\dot{m} \sim \rho_v V_B \delta L$ and $A_s \sim DL$. With the scaling $(\partial T / \partial y) \sim ((T_w - T_{sat}) / \delta)$ it can be shown that Eqs. (B6) and (B7) can be combined to eliminate δ and result in

$$V_B \sim \left(\frac{\rho_L - \rho_v \text{Ja}}{\rho_v \text{Pr}} \right)^{1/2} (gD)^{1/2} \quad (\text{B8})$$

(Ja and Pr are the Jakob and Prandtl numbers, respectively) from which t_r in Eq. (B1) is

$$t_r \sim \left(\frac{\rho_v \text{Pr}}{\rho_L - \rho_v \text{Ja}} \right)^{1/2} \left(\frac{D}{g} \right)^{1/2} \quad (\text{B9})$$

which is Eq. (18). Additionally, δ is obtained by eliminating V_B from Eqs. (B6) and (B10)

$$\delta \sim \left(\frac{k_v D_o \mu_v (T_w - T_{sat})}{h_{fg} g \rho_v (\rho_L - \rho_v)} \right)^{1/4} \quad (\text{B10})$$

Equation (B10) shows that the vapor film thickness increases as tube temperature increases (through the definition of Ja). Since δ is bounded by fixed temperatures— T_w on one side and T_{sat} on the other—the average gas temperature will increase with δ as well. This higher average gas temperature associated with increasing δ will increase the decomposition rate.

An examination of Eq. (B9) shows that increasing tube temperature increases Ja and lowers t_r because fluid moves faster through the vapor film (Eq. (B8)) as temperature increases. On this basis, one would expect that a molecule exposed to a given temperature for a shorter period of time within the film would have a lower probability of reaching vibrational states conducive to it decomposing. On the other hand, the higher temperature itself should raise the probability of decomposition. When considered in the context of Eqs. (B1) and (B4) where the product of t_r and K matters, an examination of the data in Fig. 6 shows that the flow rates of all of the stable species increased with increasing tube temperature. As such, the overriding influence on decomposition comes from the temperature in K compared to the residence time (Eq. (B9)) with its comparatively weaker dependence and opposite trend.

References

- [1] Eckhoff, R. K., 2016, "Water Vapour Explosions—A Brief Review," *J. Loss Prev. Process Ind.*, **40**, pp. 188–198.
- [2] Anderson, M. H., Meekunnasombat, P., and Corradini, M. L., 2001, "Experimental Behavior of Molten Sn/Li Impacted by a Vertical Column of Water," *Fusion Sci. Technol.*, **39**, pp. 966–969.
- [3] Vanderhaegen, M., and Le Belguett, A., 2014, "Review on Sodium Boiling Phenomena in Reactor Systems," *Nucl. Sci. Eng.*, **176**(2), pp. 115–137.
- [4] Witte, L. C., Cox, J. E., and Bouvier, J. E., 1970, "The Vapour Explosion," *J. Met.*, **22**(2), pp. 39–44.
- [5] Okuyama, K., and Iida, Y., 1994, "Film-Boiling Heat Transfer With a Catalytic Decomposition Reaction," *Jpn. Soc. Mech. Eng. Int. J., Ser. B*, **37**(1), pp. 123–131.
- [6] Zhukov, S. A., Rafeev, V. A., Afansev, S. Y., Echmaev, S. B., and Korsunksii, B. L., 2004, "Characteristic Features of the Implementation of Film Boiling of Organic Liquids," *Heat Transfer Res.*, **35**(1–2), pp. 171–179.
- [7] Epstein, M., Leung, J. C., Hauser, G. M., and Henry, R. E., 1984, "Film Boiling on a Reactive Surface," *Int. J. Heat Mass Transfer*, **27**(8), pp. 1365–1378.
- [8] Choi, S. R., Evangelista, J. W., Avedisian, C. T., and Tsang, W., 2011, "Experimental Study of Chemical Conversion of Methanol and Ethylene Glycol in a Film Boiling Reactor," *Int. J. Heat Mass Transfer*, **54**(1–3), pp. 500–511.
- [9] Kuo, W. C., Avedisian, C. T., Choi, K. W., and Tsang, W., 2014, "On Using Film Boiling to Thermally Decompose Liquid Organic Chemicals: Application to Ethyl Acetate as a Model Compound," *Int. J. Heat Mass Transfer*, **68**, pp. 456–465.
- [10] Evangelista, J. W., Avedisian, C. T., and Tsang, W., 2012, "Thermal and Catalytic Decomposition of Aqueous Ethylene Glycol Mixtures by Film Boiling," *Int. J. Heat Mass Transfer*, **55**(23–24), pp. 6425–6434.
- [11] Wang, J. P., Qian, J. M., Qiao, G. J., and Jin, Z. H., 2006, "Improvement of Film Boiling Chemical Vapor Infiltration Process for Fabrication of Large Size C/C Composite," *Mater. Lett.*, **60**(9–10), pp. 1269–1272.
- [12] Wang, J. P., Qian, J. M., Qiao, G. J., and Jin, Z. H., 2006, "Microstructure of C/C Composites Prepared by Chemical Vapor Infiltration Method With Vaporized Kerosene as a Precursor," *Mater. Sci. Eng. A*, **419**(1–2), pp. 162–167.
- [13] Zhang, Y., Gamo, M. N., and Nakagawa, K., 2002, "Synthesis of Aligned Carbon Nanotubes in Organic Liquids," *J. Mater. Res.*, **17**(9), pp. 2457–2464.
- [14] Zhang, Y., Gamo, M. N., Xiao, M. N., and Ando, C. Y. T., 2002, "Liquid Phase Synthesis of Carbon Nanotubes," *Physica B*, **323**(1–4), pp. 293–295.
- [15] Shukal, K., and Srivastava, V. C., 2016, "Diethyl Carbonate: Critical Review of Synthesis, Routes, Catalysts Used and Engineering Aspects," *RSC Adv.*, **6**(39), pp. 32624–32645.
- [16] Lewandowski, A., and Swiderska-Mocek, A., 2009, "Ionic Liquids and Electrolytes for Li-Ion Batteries—An Overview of Electrochemical Studies," *J. Power Sources*, **194**(2), pp. 601–609.
- [17] Roh, N. S., Dunn, B. C., Eyring, E. M., Pugmire, R. J., and Meuzelaar, H. L. C., 2003, "Production of Diethyl Carbonate From Ethanol and Carbon Monoxide Over a Heterogeneous Catalytic Flow Reactor," *Fuel Process. Technol.*, **83**(1–3), pp. 27–38.
- [18] Pacheco, M. A., and Marshall, C. L., 1997, "Review of Dimethyl Carbonate (DMC) Manufacture and Its Characteristics as a Fuel Additive," *Energy Fuels*, **11**(1), pp. 2–29.
- [19] Malecki, H., Deng, G., Anani, A., and Howard, J., 1999, "Thermal Stability Studies of Li-Ion Cells and Components," *J. Electrochem. Soc.*, **146**(9), pp. 3224–3229.
- [20] Domi, Y., Ochida, M., Tsubouchi, S., Nakagawa, H., Yamanaka, T., Doi, T., Abe, T., and Ogumi, Z., 2011, "In Situ AFM Study of Surface Film Formation on the Edge Plane of HOPG for Lithium-Ion Batteries," *J. Phys. Chem. C*, **115**(51), pp. 25484–25489.
- [21] Matsushita, T., Dokko, K., and Kanamura, K., 2005, "In Situ FT-IR Measurement for Electrochemical Oxidation of Electrolyte With Ethylene Carbonate and Diethyl Carbonate on Cathode Active Material Used in Rechargeable Lithium Batteries," *J. Power Sources*, **146**(1–2), pp. 360–364.
- [22] Wilke, S., Schweitzer, B., Khateeb, S., and Al-Hallaj, S., 2017, "Preventing Thermal Runaway Propagation in Lithium Ion Battery Packs Using a Phase Change Composite Material: An Experimental Study," *J. Power Sources*, **340**, pp. 51–59.
- [23] Harris, S. J., Timmons, A., and Pitz, W. J., 2009, "A Combustion Chemistry Analysis of Carbonate Solvents Used in Li-Ion Batteries," *J. Power Sources*, **193**(2), pp. 855–858.
- [24] Spotnitz, R. M., Weaver, J., Yeduvaka, G., Doughty, D. H., and Roth, E. P., 2007, "Simulation of Abuse Tolerance of Lithium-Ion Battery Packs," *J. Power Sources*, **163**(2), pp. 1080–1086.
- [25] Kim, G. H., Pesaran, A., and Spotnitz, R., 2007, "A Three-Dimensional Thermal Abuse Model for Lithium-Ion Cells," *J. Power Sources*, **170**(2), pp. 476–489.
- [26] Mandal, B. K., Padhi, A. K., Shi, Z., Chakraborty, S., and Filler, R., 2006, "Thermal Runaway Inhibitors for Lithium Battery Electrolytes," *J. Power Sources*, **161**(2), pp. 1341–1345.
- [27] Bigley, D. B., and Wren, C. M., 1972, "Pyrolysis of Carbonates—Part I: The Gas-Phase Pyrolysis of Some Symmetrical Primary Alkyl Carbonates," *J. Chem. Soc. Perkin Trans.*, **2**(2), pp. 926–928.
- [28] Mogi, R., Inaba, M., Iriyama, Y., Abe, T., and Ogumi, Z., 2003, "Study on the Decomposition Mechanism of Alkyl Carbonate on Lithium Metal by Pyrolysis-Gas Chromatography-Mass Spectroscopy," *J. Power Sources*, **119–121**, pp. 597–603.
- [29] Cross, J. T. D., Hunter, R., and Stimson, R., 1976, "The Thermal Decomposition of Simple Carbonate Esters," *Aust. J. Chem.*, **29**(7), pp. 1477–1481.
- [30] Notario, R., Quijano, J., Sanchez, C., and Velez, E., 2005, "Theoretical Study of the Mechanism of Thermal Decomposition of Carbonate Esters in the Gas Phase," *J. Phys. Org. Chem.*, **18**(2), pp. 134–141.
- [31] Gordon, A. S., and Norris, W. P., 1965, "A Study of the Pyrolysis of Methyl Ethyl and Diethyl Carbonates in the Gas Phase," *J. Phys. Chem.*, **69**(9), pp. 3013–3017.
- [32] Ritchie, P. D., 1935, "Studies in Pyrolysis—Part III: The Pyrolysis of Carbonic and Sulphurous Esters," *J. Chem. Soc.*, **400**(Pt. 1), pp. 1054–1061.
- [33] Herzler, J., Manion, J. A., and Tsang, W., 1997, "Single-Pulse Shock Tube Studies of the Decomposition of Ethoxy Compounds," *J. Phys. Chem. A*, **101**(30), pp. 5494–5499.
- [34] Lienhard, J. H., IV, and Lienhard, J. H., V, 2003, *A Heat Transfer Textbook*, 3rd ed., Phlogiston, Cambridge, MA, pp. 429–431, 468, 483–486.
- [35] Special Metals, 2008, "Inconel Alloy 600," Special Metals Corp., Huntington, WV, accessed Dec. 7, 2017, <http://www.specialmetals.com/assets/smc/documents/alloys/inconel/inconel-alloy-600.pdf>
- [36] Bradfield, W. S., 1966, "Liquid-Solid Contact in Stable Film Boiling," *Ind. Eng. Chem. Fundam.*, **5**(2), pp. 200–204.
- [37] Dhuga, D. S., and Winterton, R. H. S., 1986, "Measurement of Liquid-Solid Contact in Boiling," *J. Phys. E: Sci. Instrum.*, **19**(1), pp. 69–75.
- [38] Kikuchi, Y., Ebisu, T., and Michiyoshi, I., 1992, "Measurement of Liquid-Solid Contact in Film Boiling," *Int. J. Heat Mass Transfer*, **35**(6), pp. 1589–1594.
- [39] Chang, K. H., and Witte, L. C., 1990, "Liquid-Solid Contact During Flow Film Boiling of Subcooled Freon-11," *ASME J. Heat Transfer*, **112**(2), pp. 465–471.
- [40] Avedisian, C. T., 1985, "The Homogeneous Nucleation Limits of Liquids," *J. Phys. Chem. Ref. Data*, **14**(3), pp. 695–720.
- [41] Park, J., Zhu, R. S., and Lin, M. C., 2002, "Thermal Decomposition of Ethanol—I: *Ab Initio* Molecular Orbital/Rice–Ramsperger–Kassel–Marcus Prediction of Rate Constant and Product Branching Ratios," *J. Chem. Phys.*, **117**(7), pp. 3224–3231.
- [42] Amran, T., Abdullay, T., and Croiset, E., 2014, "Evaluation of an Inconel-625 Reactor and its Wall Effects on Ethanol Reforming in Supercritical Water," *Ind. Eng. Chem. Res.*, **53**(6), pp. 2121–2129.
- [43] Bromley, L. A., 1950, "Heat Transfer in Stable Film Boiling," *Chem. Eng. Prog.*, **46**(5), pp. 221–227.
- [44] Urban, B. J., Avedisian, C. T., and Tsang, W., 2006, "The Film Boiling Reactor: A New Environment for Chemical Processing," *AIChE J.*, **52**(7), pp. 2582–2595.
- [45] Benson, S. W., 1960, *The Foundation of Chemical Kinetics*, McGraw-Hill, New York, Chap. 11.